AD-A035 938 MASSACHUSETTS INST OF TECH CAMBRIDGE DEPT OF EARTH A--ETC F/G 8/7
NEAR SURFACE ELECTRICAL PROPERTIES OF ROCKS AS A GUIDE TO MECHA--ETC(U)
DEC 76 T R MADDEN, E WILLIAMS F19628-76-C-0070
UNCLASSIFIED AFGL-TR-76-0305 NL

| OF |
AD
A035938

END

DATE
FILMED
3-77

AFGL-TR-76-0305

NEAR SURFACE ELECTRICAL PROPERTIES OF ROCKS AS A GUIDE TO MECHANICAL PROPERTIES

Massachusetts Institute of Technology
Department of Earth and Planetary Sciences
Cambridge, Massachusetts 02139

Theodore R. Madden
Earl Williams

Final Report

Period Covered: October 1, 1975 - September 30, 1976

Date of Report: December 31, 1976

AIR FORCE GEOPHYSICS LABORATORY
AIR FORCE SYSTEMS COMMAND
UNITED STATES AIR FORCE
HANSCOM AFB, MASSACHUSETTS 01731

Unclassified

SECURITY CLASSIFICATION OF THIS PAGE (When Data Entered)

REPORT DOCUMENTATION PAGE	READ INSTRUCTIONS BEFORE COMPLETING FORM
1. REPORT NUMBER: AFGL-TR-76-0305	2. GOVT ACCESSION NO. / 3. RECIPIENT'S CATALOG NUMBER
4. TITLE (and Subtitle): NEAR SURFACE ELECTRICAL PROPERTIES OF ROCKS AS A GUIDE TO MECHANICAL PROPERTIES.	5. TYPE OF REPORT & PERIOD COVERED: Final rept. 1 Oct 75 - Oct. 1, 1975-Sept.30,1976 (30 Sep 76)
	6. PERFORMING ORG. REPORT NUMBER
7. AUTHOR(s): Theodore R. Madden, Earl Williams	8. CONTRACT OR GRANT NUMBER(s): F19628-76-C-0070 new
9. PERFORMING ORGANIZATION NAME AND ADDRESS: Mass. Inst. of Technology, Dept of Earth and Planetary Sciences, Cambridge, Massachusetts 02139	10. PROGRAM ELEMENT, PROJECT, TASK AREA & WORK UNIT NUMBERS: 62101F, 7639 1301, 13
11. CONTROLLING OFFICE NAME AND ADDRESS: Air Force Geophysics Laboratory, Hanscom AFB, Massachusetts 01731, Monitor/LWH/Lt Mark Settle	12. REPORT DATE: 31 Dec 76 / December 31, 1976
	13. NUMBER OF PAGES: 45 (47 p.)
14. MONITORING AGENCY NAME & ADDRESS (if different from Controlling Office)	15. SECURITY CLASS. (of this report): Unclassified
	15a. DECLASSIFICATION/DOWNGRADING SCHEDULE

16. DISTRIBUTION STATEMENT (of this Report)

Approved for public release; distribution unlimited.

ACCESSION for	
NTIS	White Section ☐
DDC	Buff Section ☐
UNANNOUNCED	☐
JUSTIFICATION	
BY	
DISTRIBUTION/AVAILABILITY CODES	
Dist.	AVAIL. and/or SPECIAL
A	

17. DISTRIBUTION STATEMENT (of the abstract entered in Block 20, if different from Report)

18. SUPPLEMENTARY NOTES

19. KEY WORDS (Continue on reverse side if necessary and identify by block number)

cracks, rocks, electrical, mechanical, properties

20. ABSTRACT (Continue on reverse side if necessary and identify by block number)

The intense crack production that occurs in highly stressed rocks greatly increases the interconnectivity and the conductivity efficiencies of the cracks. Network models of this effect give reasonable estimates of the electrical properties. The surface conductivity contribution is still modest and limits the range of zeta potentials. Turbulence effects are shown to reduce the experimental determinations of these potentials. Extensions of the network models are made to treat the mechanical effects of the

OVER

DD FORM 1 JAN 73 1473 EDITION OF 1 NOV 65 IS OBSOLETE

404 784

SECURITY CLASSIFICATION OF THIS PAGE (When Data Entered)

interconnected cracks, but the application of the method is still incomplete.

Introduction

In our earlier studies, summarized in the final report for AFCRL-TR-75-0179 (Madden, 1974), it was shown that for relatively competent rocks in the near surface there were divergencies between the trends of the electrical and mechanical properties. This was believed to be due to the strong influence of joints and faults on the elastic properties as compared to the microcrack control of the electric properties. Their differences become reduced for rocks which have been weakened by stress cycling, which we believe is due to the increased influence of microcracks on elastic as well as electric properties in such rocks. This present study has thus concentrated on developing a better quantitative understanding of how the developing microcrack population that is associated with highly stressed rocks effects the electrical and mechanical properties of such rocks. Our approach has been to extend our earlier work on random networks and its application to the electrical properties of the microcrack structure in order to investigate the role of an increasing crack population on these electrical properties. We have also started to extend the application of these concepts to include mechanical properties. A most important problem in this area is that concerned with crack development under stress and the onset of failure. This is a much more difficult problem since it is essentailly non-linear, but one which we believe is well suited to our random network approach.

In the first section we investigate the modifications in our theory of the electrical conductivity of an interconnected crack system that is necessary to account for the effects of increasing the crack population. New cracks introduced into a system of already interconnected cracks play a very different role than the original cracks and cause a remarkable increase in the electrical conductivity. These concepts also expose a similar effect that results from interactions between cracks of different length scales. In the second section we extend our earlier work on streaming potential measurements and analysis in order to try and clarify the role of surface conductivity in rock electrical properties. In the third section we introduce the principals needed for making network approximations of elastic properties. The fourth section was to be concerned with the application of random networks to the rock failure problem. The numerical studies are not complete enough to report on here, and will be reported later. The work is far from complete but holds promise for greatly aiding our quantitative understanding of failure and rock strength properties. The last section summarizes our conclusions about the interconnection between electrical and mechanical properties.

I

Microcrack Electrical Conductivity Effect of Stress Induced Cracks

Introduction

In our final report of project 7639 we outlined a theory which can be used for predicting the electrical conductivity of porous media given the distribution function of the porous zone widths. This theory could be an important breakthrough in gaining a quantitative understanding of rock electrical properties, but it needs testing on real materials. Data provided by Kate Hadley (Hadley, 1975) on the crack parameter distribution functions of stressed and unstressed Westerly granite should provide us with the opportunity of testing and improving the theory.

Figure 1 shows the crack width distribution functions determined from electron scanning microscope examination of surfaces of Westerly granite which had undergone various degrees of stressing. This figure clearly shows the large increase in crack density created by stressing, and also shows an increase weighting towards the narrower cracks as the stress levels increased. The narrowest cracks could not be seen by the scanning microscope because of the coating used, so the .0055 and .0017μ distributions have been inferred by extrapolation. In the unstressed rocks the distribution function is decreasing beyond .173μ, but the stressed rocks show increasing densities up to the limit of resolution of the scanning microscope which is about .03μ.

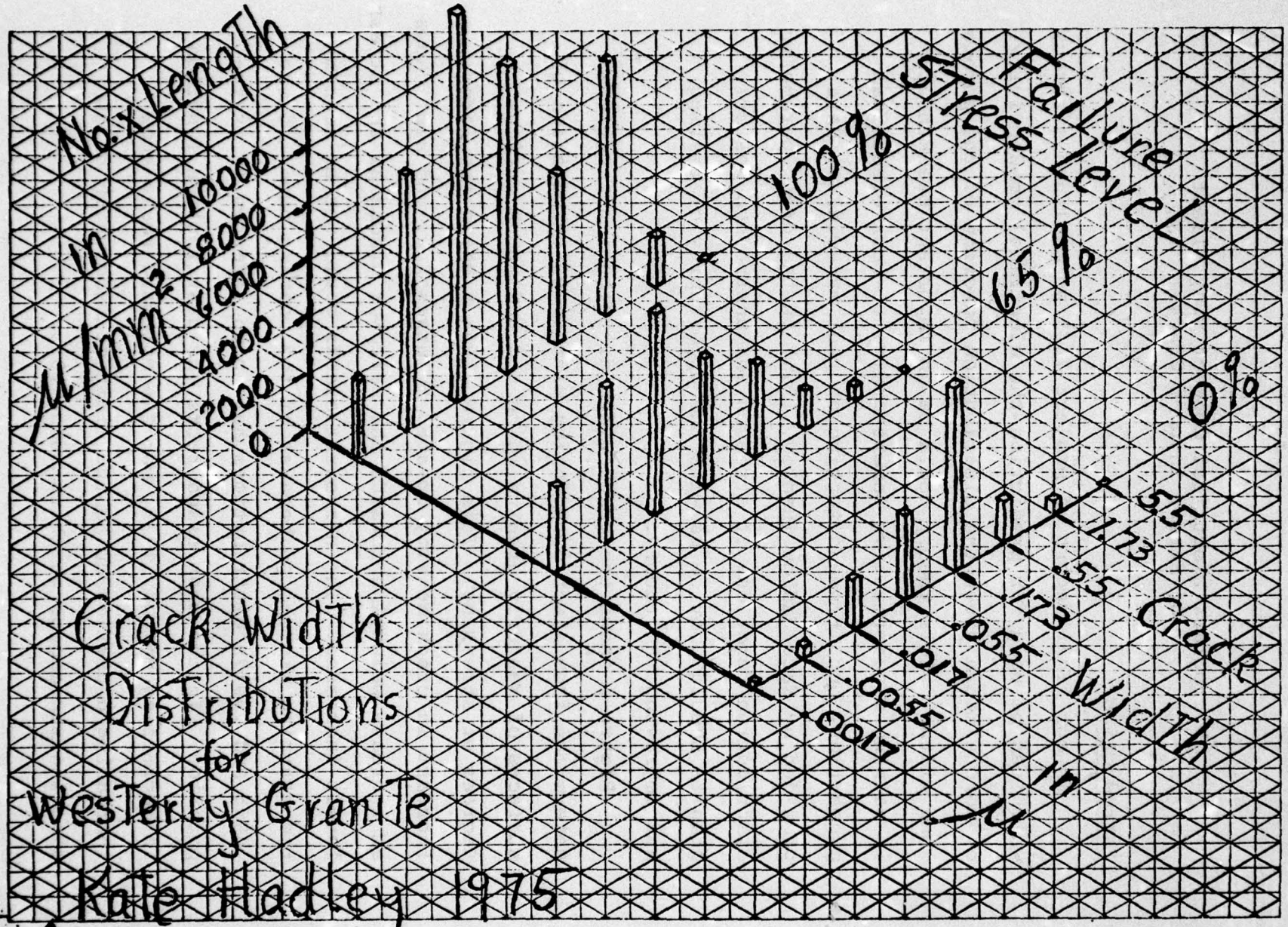
No. x Length
in
μm
mm²
10000
8000
6000
4000
2000
0
Failure
Stress Level
100%
65%
0%
.55
.173
.055
.017
.0055
.0017
Crack
Width
in
μm
Crack Width
Distributions
for
Westerly Granite
Kate Hadley 1975

Fig 1

Conductivity Theory

Our previous studies of random network models of porous zone conduction paths indicated that different networks gave quite similar results when the distribution function of the element values was smooth. They further showed that the geometric mean was a good estimate of the final conductivity in such cases.

$$Y = \prod_i Y_i^{P_i} \tag{1}$$

In these network models the element conductances were equal to the conductivity of the zone being represented by the element and thus proportional to the width of the porous zone involved. This width also determines the porosity contribution of the porous zone. The width however does not influence the frequency of occurrence of the porous zones (which we assume are more crack like than tube like) and therefore we have

$$P(w_i) = \frac{\phi_i / w_i}{\sum_j (\phi_j / w_j)} \tag{2}$$

w_i = width i

ϕ_i = porosity associated with w_i

$P(w_i)$ = probability of elemental conduction path having width w_i

Since the conductivity of the elemental zones is proportional to its width one should have a proportionality between porosity and conductivity which might be given as

$$\phi_i = P(w_i) Y_i / \sigma_{fluid} \qquad (3)$$

From (2) and (3) we would then infer

$$Y_i = \sigma_{fluid} w_i \sum_j (\phi_j / w_j) \qquad (4a)$$

This result needs some adjustment, however, since a constant width distribution would give a resultant conductivity equal to the fluid conductivity x porosity. This would only be true if all the crack and pore zones were aligned parallel to the current flow, and is the result of not properly accounting for the volume associated with conduction paths aligned perpendicular to the current flow. The case of a single width distribution should optimize the total conductivity and lead to a result close to the Hashin upper bound. Using this result as a correction factor we would modify (4a) to

$$Y_i = \sigma_{fluid} [(2/(3-\phi)) w_i \sum_j (\phi_j / w_j)] \qquad (4b)$$

$$\phi = \text{total porosity} = \sum_j \phi_j$$

Given the crack or pore zone width distribution as $\phi_j(w_j)$ one can arrive at a conductivity estimate using (4b), (2), and (1). The surface conductivity effect can also be included by adding to each Y_i an appropriate fraction that

represents the surface conductivity contribution relative to the pore fluid contribution. Table I shows the resultant parameters that apply to the unstressed Westerly granite assuming a zeta potential of 75 mv.

Table I

Crack Conductivity Parameters for Westerly Granite

Crack Width in μ	Prob (w_i)	$Y(w_i)/\sigma_{fluid}$ Saturated NaCl	$Y(w_i)/\sigma_{fluid}$ 10^{-3} N NaCl
5.5	.003	.0555	.0566
1.7	.030	.0171	.0182
.55	.097	.00555	.00649
.17	.439	.00171	.00266
.055	.225	.000555	.00150
.017	.117	.000171	.00111
.0055	.059	.0000555	.000555
.0017	.020	.0000171	.000171

Using 50 Ω-M for the 10^{-3}N fluid resistivity, we predict a resistivity of 24,000 Ω-M for the granite and a formation factor of 1143 which results in an effective fluid resistivity of 21 Ω-M. This can be compared to Brace's measurements extrapolated to zero pressure (Brace et al, 1965) on Westerly granite which gave an average resistivity of 7,000 Ω-M and a formation factor of 614 which results in an effective fluid resistivity of 11 Ω-M. The formation factors are in rough agreement. The larger difference in the resistivities with dilute solutions may reflect an error in the experimental data. The observed apparent fluid

resistivity of 11 Ω-M seems difficult to explain by surface conduction with reasonable zeta potentials and suggests that the pore fluids were somewhat contaminated.

A check on this was made by a series of experiments on Westerly granite that attempted to eliminate any previous salt contamination. Two approaches were used. In one, samples were placed in distilled water to allow diffusion of the contamination out of the sample. This is a slow procedure and there is some possibility that the highly oxidizing environment in the laboratory owuld cause some decomposition of the samples. After an apparent steady state was reached the samples were resaturated with 10^{-3}N solutions and their resistivity measured. This procedure only resulted in modest changes in the resistivity, from 7,000 Ω-M before desalting to 10,000 Ω-M after. A more satisfactory approach was to decontaminate the samples by flushing, as a steady state was reached on a much shorter time scale. This treatment significantly increased the rock sample resistivities, up to 18,000 Ω-M, and conclusively showed that the samples were originally contaminated.

The porosity of these cracks amounts to only 0.32% which is considerably less than the total porosity, which is typically 1% for Westerly granite. Large cracks would have only a small chance of having been intercepted in the area of only .45mm^2 used in the crack study. The number density of any such large cracks would be so low, however, that as long as they do not form an interconnected set by themselves, they would only lower the predicted resistivity by a few percent.

Complications of the Simple Model

When the same procedure is applied to the data on the stressed rocks very poor predictions are obtained. The great increase in the relative number density of the very narrow cracks offsets the effect of an increase in the total crack porosity and in one case an actual lowering of the rock conductivity is predicted. There is an obvious shortcoming to the procedures outlined above when applied to these stressed rocks, which points out a necessary modification of the theory.

The stressed rocks have a new crack population which is added on to the preexisting population. Obviously the new cracks have certain topological restrictions relative to their interactions with the preexisting cracks. These restrictions are ignored, however, when the whole population is lumped together. Thus, for instance, no new crack can act in series between two previously connected cracks. Something similar must also be taken into account when considering interactions between cracks of different length scales. The cascading process that is the essence of our random network models allows interactions between different size scales, but only by cascading from one scale to the next. This concept is valid for three dimensional zones as different scale sizes cannot interact directly since they occupy different volumes. Cracks and pore zones are essentially two dimensional however and different scale sizes can occupy the same volume and thus interact directly. The cascading process tends towards the

geometric mean which is a compromise between series and parallel interactions, but direct interactions are more parallel like.

We can take account of direct interactions between scale sizes by allowing interconnected zones of one scale to act in parallel with individual elements of the next larger scale as shown in Figure 2. Using the symbol << >> for the random network type averaging which we approximate by the geometric mean and indicating scale size by superscripts we have

$$Y = <<...<<Y^{\gamma} + <<Y^{\beta} + <<Y^{\alpha}>> >> >>...>> \qquad (5)$$

$$\gamma \text{ scale} > \beta \text{ scale} > \alpha \text{ scale}$$

The same sort of procedure must also be used to consider the interaction of the new cracks with respect to the pre-existing ones. At each scale level the new cracks must be considered acting somewhat in parallel with the old cracks. Since the process indicated in equation (5) greatly decreases the effective width of the conductivity distribution at any length scale an approximation to the new and old crack interaction is given by

$$Y = <<...<<Y^{\gamma}_{new} + <<Y^{\gamma}_{old} + <<Y^{\beta}_{new} + <<Y^{\beta}_{old} + \qquad (6)$$

$$<<Y^{\alpha}_{new} + <<Y^{\alpha}_{old}>> >> >> >>...>>$$

$$\gamma \text{ scale} > \beta \text{ scale} > \alpha \text{ scale}$$

The use of equation (6) requires the knowledge of the length as well as the width distribution of the cracks, and

$$\ll y^i \gg + \ll y^{i-1} \gg \leq \ll y^i + \ll y^{i-1} \gg \gg \leq \ll y^i + y^{i-1} \gg$$

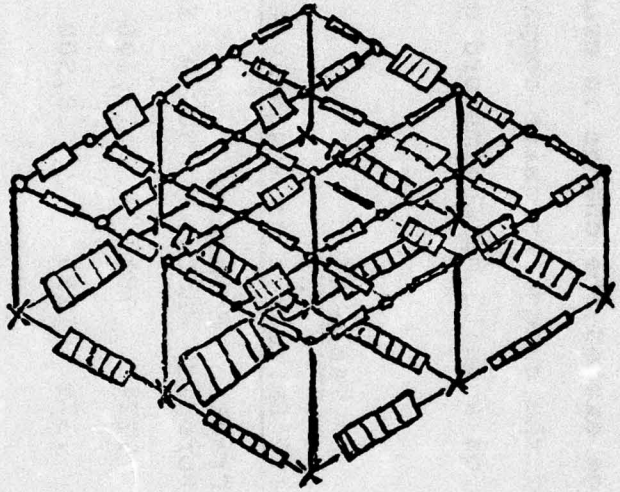

Interaction of Conduction Paths of Different Length Scales

Fig 2

the identification of the old and new crack populations. For stressed samples the prestress crack population had to be estimated from the data on the usntressed sample. These breakdowns are shown in Figures 3, 4, and 5. The results of equation (6) applied to this data are given in Table II. These results show that the changes in electrical conductivity due to stress damage exceed the change in crack porosity. The actual magnitude of the change is quite comparable to the values we obtained on a suite of Chelmsford granites as reported previously.

Table II

Conductivity Estimates on Westerly Granite

Sample	Crack Porosity	Formation Factor	$\rho_{effective}$ (50Ω-M fluid)	$\rho_{effective}$ of fluid
Unstressed	.32%	783	19,100	24.4
T5 prestressed (assumed)	.37%	1250	28,500	22.8
T5 stressed to 65% of failure	.40%	1010	18,700	18.5
W5 prestressed (assumed)	.32%	900	25,200	28
W5 stressed to 100% of failure	.96%	245	6,420	26.2

The predicted conductivity for the unstressed sample was also brought more in line with laboratory measurements by the extensions outlined above.

These rocks also posess a further porosity not sampled in the crack data. Large cracks and pores could have been missed in the small area used for the crack study. but such paths would have such low probabilities relative to their volumes that their contribution to the rock conductivity is minor provided they do

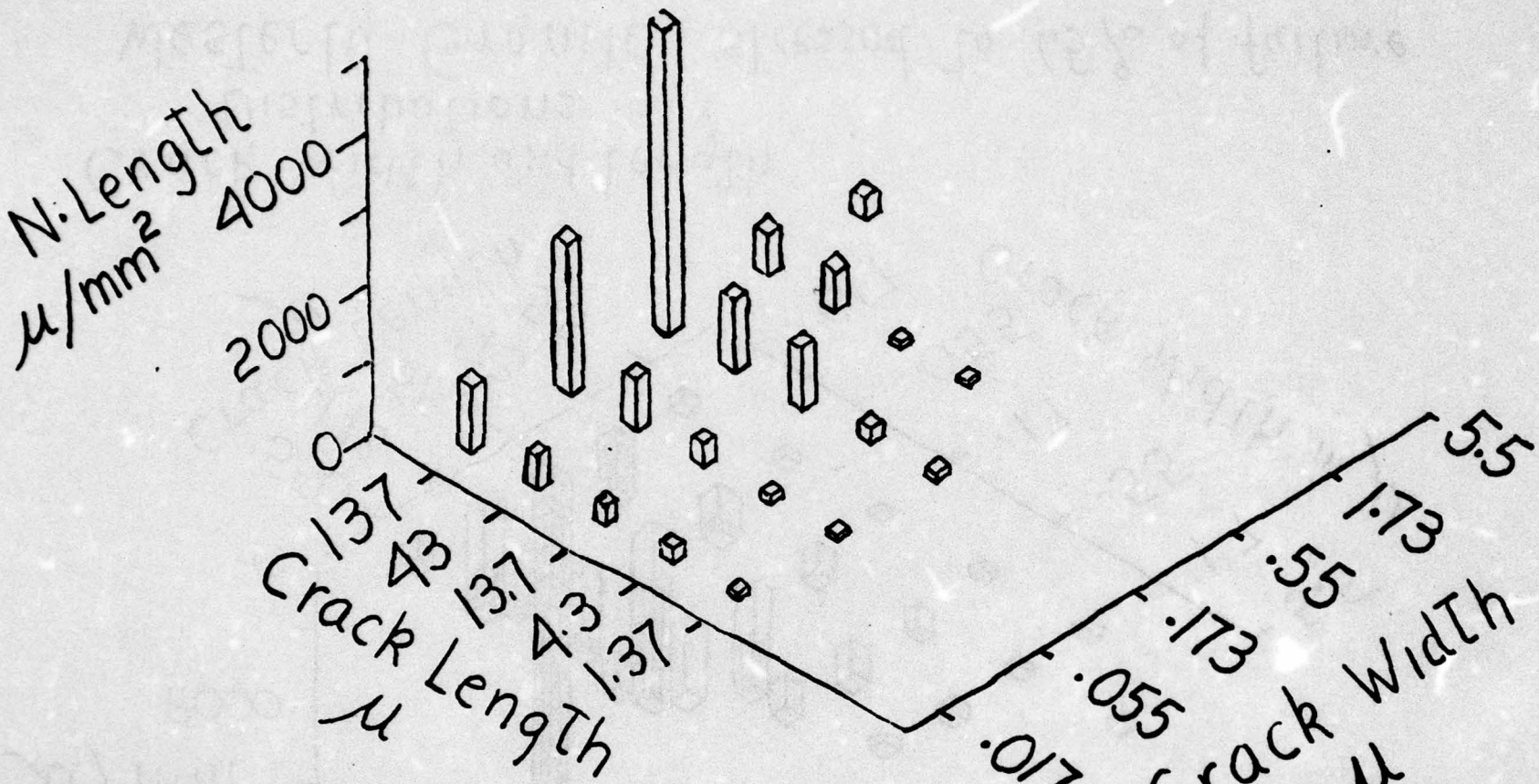

Crack Width and Length
Distributions
Westerly Granite unstressed

Fig 3 (K. Hadley 1975)

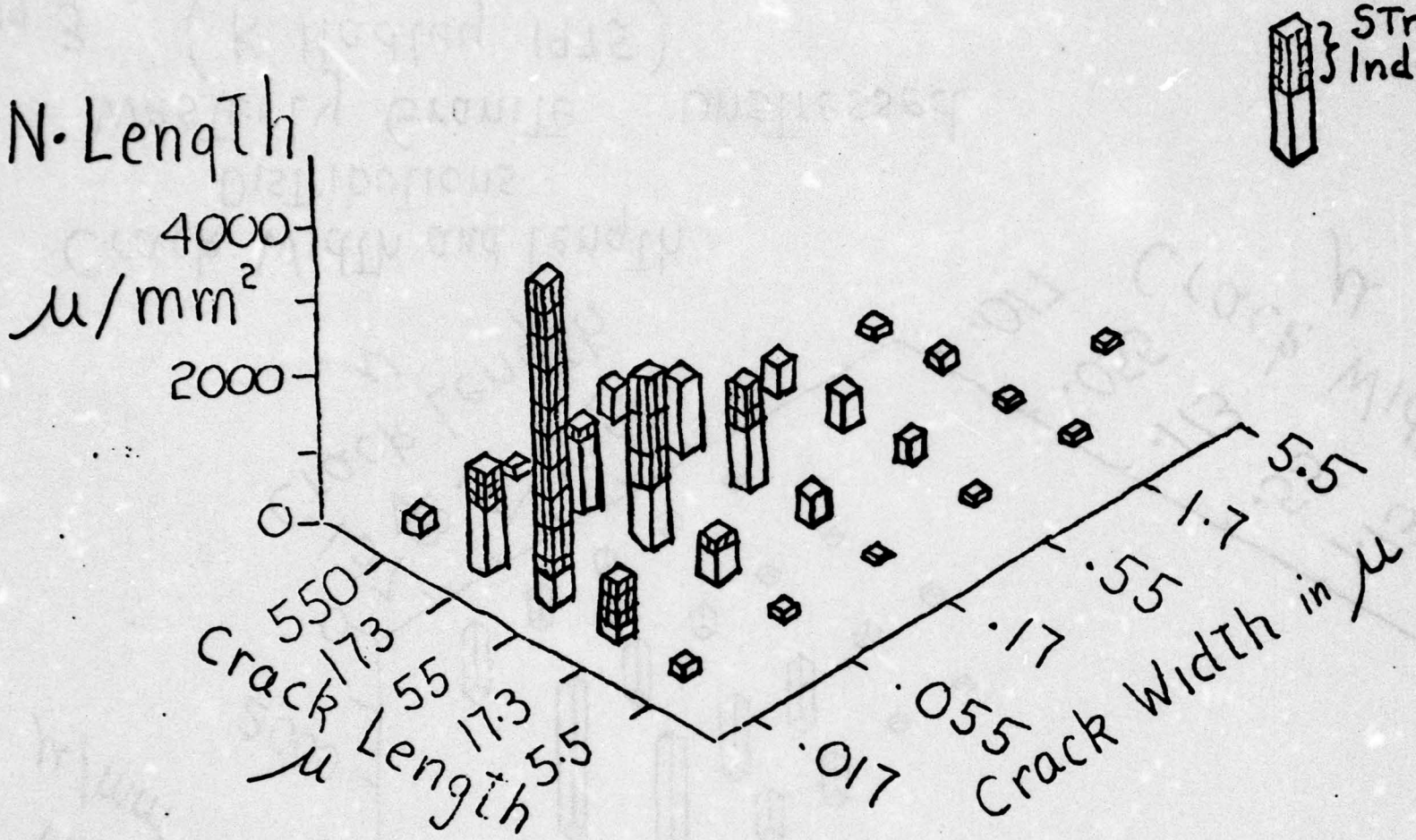

Crack Width and Length Distributions
Westerly Granite stressed to 65% of failure
(K. Hadley, 1975)

Fig 4

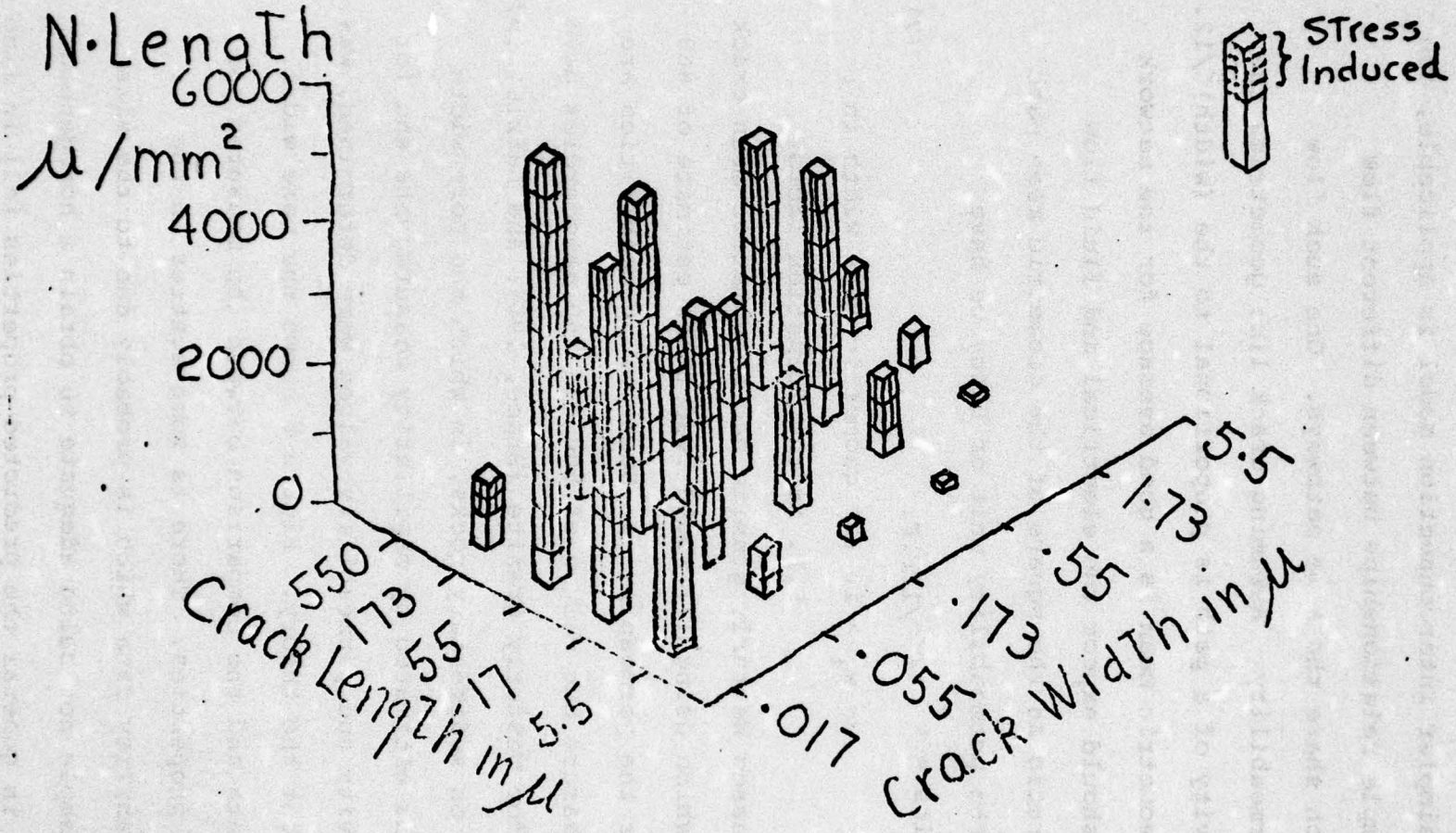

Crack Width and Length
Distributions
Westerly Granite stressed to 100% of failure
(K. Hadley, 1975)

Fig 5

not form an interconnected system by themselves.

When the simpler interconnection model is applicable, one should find simple relationships between different flow properties which share the same pathways. One such flow property is permeability. Assuming crack like geometries the fluid conductivity of a path is proportional to the $(\text{width})^3/12$. Whenever the geometric mean is a good average for the network properties we should expect the electrical and fluid flow properties to ratio as the square of the geometric mean path width. Using the permeability unit of Darcy we have

$$k \text{ in darcies} = \langle\langle w_i^2 \rangle\rangle / 12 F.F. \qquad (7)$$

$\langle\langle w_i \rangle\rangle$ is the geometric mean width in μ

F.F. is the formation factor

The unstressed Westerly granite had a geometric mean crack width of .09μ which using (7) would lead to an estimate of 860 nanodarcies for the permeability. Such low permeabilities are difficult to measure but values of 500 and 750 nanodarcies have been reported for Westerly granite (Brace, 1968, and Batzle, 1976).

Some data on sedimentary rocks, in which the pore width distribution was estimated by capillarity measurements and for which conductivity and permeability values were determined, was also used to test the theory. Figure 6 shows the pore width distribution data and the comparison between the measured and predicted flow properties. There is some scatter in the measured peremability data which is probably due to the size scale of the sample not being adequate to obtain a homogeneous averaging, but in general the predicted properties fall in line with the measured values.

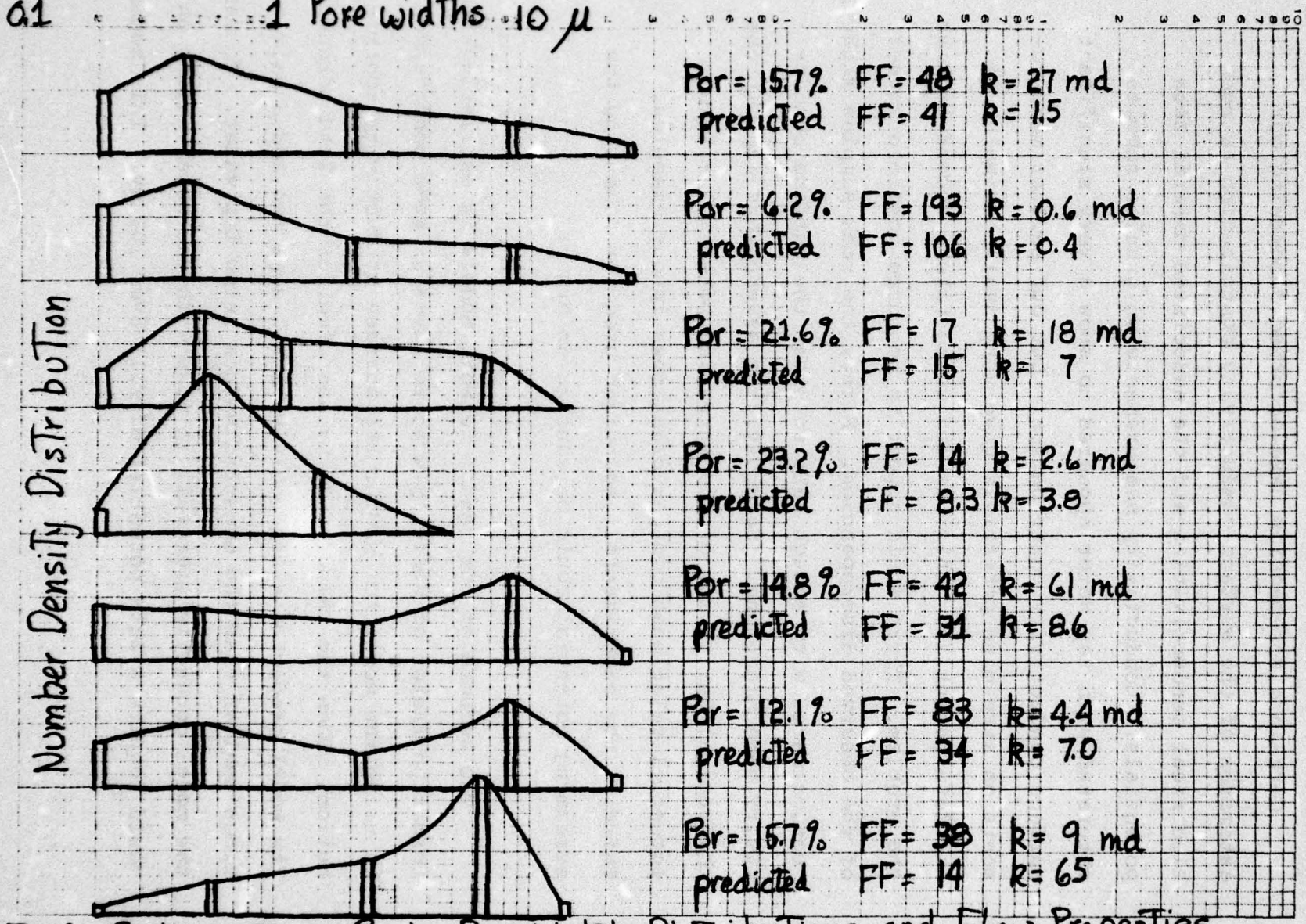

Fig 6 Sedimentary Rock Pore Width Distributions and Flow Properties

II

Zeta Potentials Reexamined

Certain discrepancies have occurred concerning our estimates of the surface conductivity contribution to rock electrical conductivities and the associated mineral Zeta potentials. Conductivity measurements on granite samples saturated with tap water appeared to show a very significant surface conductivity contribution, but our earlier measurements on streaming potentials gave very small estimates of the Zeta potential. This has led us to take a second look at the problem. There would appear to be three possible causes of the observed discrepancies. First, the rock samples might be contmainated with enough salt to upset the surface conductivity determinations. Secondly, the assumptions made in the theoretical derivation of the streaming potential - Zeta potential relationship might break down in our examples. Thirdly, the experimental technique used for measuring the streaming potential could be causing an error.

The success of our random network models in estimating the formation factor of Westerly granite gives us some confidence in using the model to examine the surface conductivity contribution. When the value of 75 mv was used for the Zeta potential, the model predicted a conductivity still some two and a half times smaller than the measured values using tap water. To make the model conductivities fall in line with the observations one would require a Zeta potential of well over 100 mv. This seems

like an unlikely value and therefore we examined the possibility of salt contamination.

Figure 7 shows the results of diffusion experiments for granite samples immersed in distilled water. The 15,000 OHM meter value reached after 90 days is probably too low for a distilled water saturation, and is indicative of the slow diffusion through rocks. The effective diffusivity of a rock is proportional to its electrical conductivity, but the volume participating in the diffusion is given by the porosity. Thus the effective length of the diffusion paths are their actual length x formation factor x porosity. For Westerly granite the effective length is about a factor of 10 greater than the actual length so that the diffusion time for one centimeter penetration in about 100 days.

When these samples were dried by evaporation and resaturated in tap water the resistivity was reduced to 10,200 Ω-M. Since the salts left in the rock after the diffusion experiment were still present, this result indicated the tap water saturated samples should have considerably higher resistivities.

Subtracting off the conductivity contribution remaining after the diffusion experiment leaves 30,000 Ω-M as the tap water component of the resistivity. One still cannot untangle with this data the surface conductivity contribution from the salt contamination, however.

Finally, a series of experiments were carried out using hydraulic flushing that gave consistent results and firmly establish the influence of contamination on the earlier measurements. Using permeability measuring apparatus, distilled

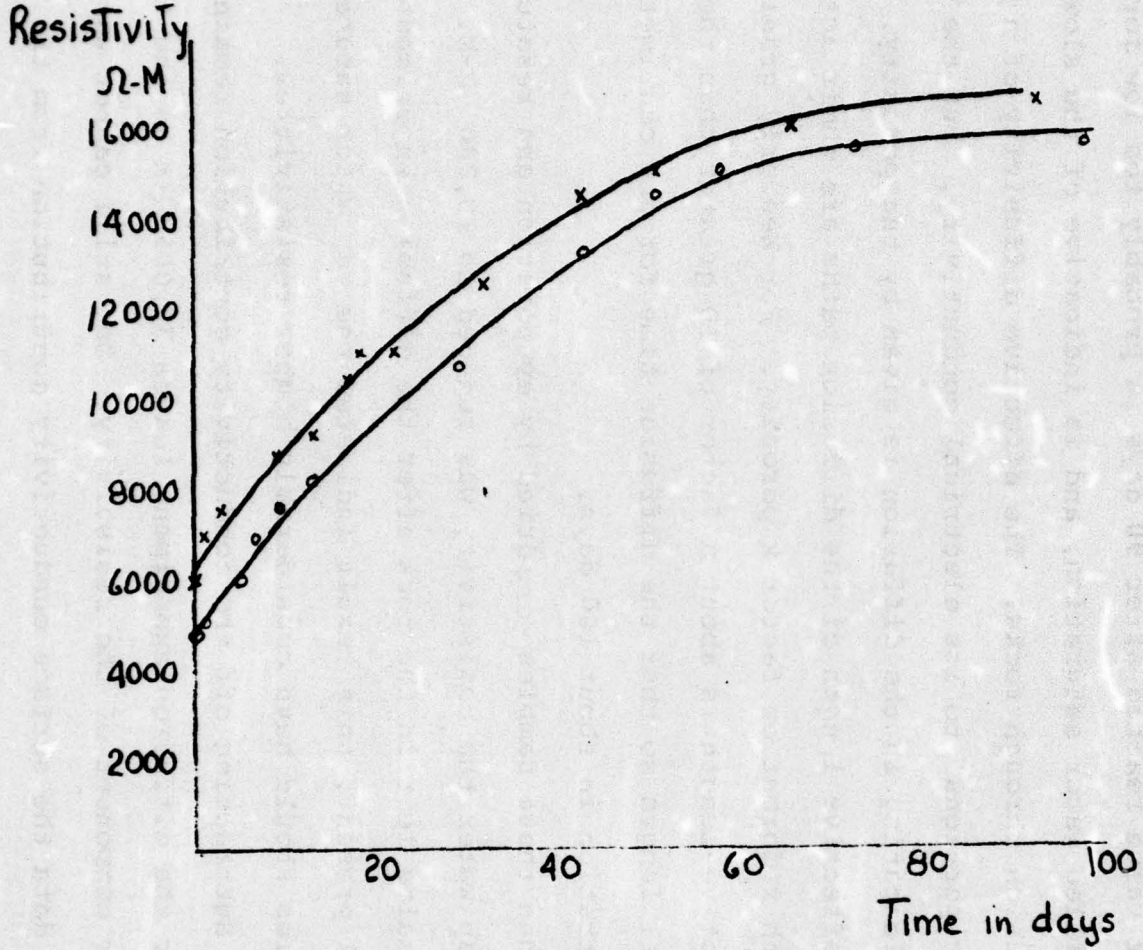

Fig 7 Resistivity of Westerly Granite Samples
Soaked in distilled water

water was forced through a Westerly granite sample about 2 cm thick by a 50 bar pressure. Over a period of thirteen days, the resistivity increased from 10,000 Ω-M to 30,600 Ω-M. On saturating the flushed out sample with tap water the resistivity went to 18,000 Ω-M. Forcing the tap water (equivalent to 10^{-3} N salt solution) through the sample for an additional fifteen days did not change the resistivity appreciably.

TABLE III

Desalting Experiments on Westerly Granite

Resistivity	Treatment
6,000 Ω-M	tap water saturation
10,200	diffusion flushing (100 days) and resaturating
18,800	distilled water flow flushing (13 days) and resaturating
18,000	tap water flow flushing (15 days)

As mentioned in the first chapter a Westerly granite resistivity of 18,000 Ω-M with tap water saturation is quite compatible with an effective Zeta potential of 75 mv. None of our earlier attempts to determine the Zeta potential from streaming potential measuremetns gave results anywhere as near as large as this value. Table IV reviews some of these older measurements and also includes more examples. These measurements were made on crushed samples using about one or two atmospheres of pressure drive.

Table IV

Streaming Potential Measurement Results

on

Crushed Samples Using 1-2 Atmospheres Pressure

Sample (Solution) Minerals	$\frac{\partial \upsilon}{\partial p}$ mv/bar	ϕ_o (mv)
Feldspar (tap water)	38	11
" "	69	17
" "	57	19
" "	80	23
"(10^{-3} Nacl)	210	36
"(10^{-2}Nacl)	12	20
"(10^{-3}Nacl)	64	11
"(10^{-2}Nacl)	13	21
Quartz (tap water)	60	19
" "	49	13
"(10^{-3}Nacl)	159	27
"(10^{-2}Nacl)	12	20
Mica (tap water)	46	13
" "	57	17
Rocks		
Answan Granite (tap water)	38	11
Biotite Granite	60	17
Westerly Granite	68	19
Chelmsford Granite	64	18
" "	86	24
"(10^{-3}Nacl)	237	40
"(10^{-2}Nacl)	30	50

At first we thought that limitations in the streaming potential theory could be at fault. The usual theory assumes a Piosseuille flow drags the diffuse layer setting up a potential which causes a counter electric flow which just balances the convected electric flow. The effect on the fluid flow due to the electric field is ignored. This effect can be incorporated in the theory, however, by adding an electric drag force, ρE, to the Navier-Stokes equation

$$\eta\frac{d^2v(x)}{dx^2} + \rho(x)E = -\nabla P \qquad 2.1$$

the space change, ρ , which is convected by the flow is determined by Poisson's equation

$$\rho(x)=-\varepsilon\frac{d^2\phi(x)}{dx^2} \qquad 2.2$$

Using 2.2 and 2.1 and the boundary conditions

$$\frac{dv}{dx}\Big|_{x=0} = 0 \qquad v\Big|_{x=\pm R} = 0 \qquad 2.3$$

we obtain by integration the velocity profile

$$v(x) = \frac{\nabla P}{2\eta}(x^2-R^2) - \frac{\varepsilon E}{2\eta}\left[\phi(R)-\phi(x)\right] \qquad 2.4$$

The potential ϕ can be determined form Poisson's equation (2.2) and the Boltzmann equation

$$\eta_+=\eta_\circ e^{-\phi/kT}$$
$$\eta_-=\eta_\circ e^{\phi/kT}$$
$$\rho=Z_+\eta_+-Z_-\eta_- \qquad 2.5$$

In the case of a single binary ion pair this has an exact solution

$$\left(\frac{e^2}{\varepsilon kT}\ \Sigma\eta_{i0}Z_i^2\right)^{1/2} X=\ln\ \frac{(e^{ZE\phi/2kT}+1)(e^{Ze\phi_\circ/2kT}-1)}{(e^{Ze\phi\ /2kT}-1)(e^{ZE\phi_\circ/2kT}+1)} \qquad 2.6$$

$\phi_\circ = \phi(x=0)$ Zeta potential 2.7

with $\frac{d\phi}{dx} = 2\left(\frac{2\eta kT}{\varepsilon}\right)^{1/2} \sinh\left(\frac{Ze\phi}{2kT}\right)$ 2.8

From these results a more exact streaming potential theory can be developed. The convection current due to the fluid motion is

$$i_{convection} = \int_{-R}^{R} \rho(x) v(x) dx \qquad 2.9$$

which from 2.2 and 2.4 can be written

$$i_{convection} = \int_{-R}^{R} \left\{ -\frac{\varepsilon \nabla P}{2\eta} (X^2 - R^2) \frac{d^2\phi}{dx^2} + \frac{\varepsilon^2 E}{\eta} \left(\phi(R) - \phi(x) \frac{d^2\phi}{dx^2}\right)\right) dx \qquad 2.10$$

Integrating by parts and using the boundary conditions 2.3 and 2.7

$$i_{convection} = - \frac{\varepsilon \nabla P 2R\phi_o}{\eta} - \frac{\varepsilon \nabla P}{\eta} \int_{-R}^{R} \phi(x) dx + \frac{\varepsilon^2 E}{\eta} \int_{-R}^{R} \left(\frac{d\phi}{dx}\right)^2 dx \qquad 2.11$$

The last term is the modification due to the electric drag on the fluid. Using tap water parameters we find that this term is not important as long as the channel widths, 2R, are large compared to a Debye length (.01μ). This same restriction applies to ignoring the second term in (2.11) and also to ignoring the surface conductivity contribution to the conduction current. We used crushed samples in order to make the channel widths large and thus we would not predict any difficulty with the usual streaming potential theory. This simpler theory gives the result

$$E/\nabla p = \varepsilon \phi_o / \eta \sigma \qquad 2.12$$

The use of wide channels avoids a difficulty due to surface conduction, but it opens up the possibility of a different problem, turbulence. The turbulence regime is associated with high

Reynolds numbers. The Reynolds number is defined as

$$R = \rho v d/\eta \qquad 2.13$$

where ρ stands for fluid density

v mean flow velocity

d channel width

η viscosity

Assuming Poisseuille flow we can rewrite (2.13) in terms of the applied pressure gradients

$$R=\frac{1}{12}\ \frac{\Delta P}{L}\ \frac{\omega^3\rho}{\eta^2} \qquad \text{for cracks width = w length = L} \qquad (2.14a)$$

$$R= \frac{1}{4}\ \frac{\Delta P}{L}\ \frac{R^3\rho}{\eta^2} \qquad \text{for tubes radius = R length = L} \qquad (2.14b)$$

For tubes the critical Reynolds number is between 2000 and 60,000 and for two dimensional channels it is between 900 and 5,000. It seems reasonable to expect turbulence to be set up more easily, however, when the pathways are uneven and tortuous. Using typical values pertaining to the measurements reported in Table IV,

$$\frac{\Delta P}{L} = 5\times10^5 \ \text{Newtons/M}^3$$

$$\rho = 10^3 \ \text{Kgm/M}^3$$

$$\eta = 10^{-3} \ \text{Newton-sec/M}^2$$

we should expect turbulence to be well developed for widths of 200-300μ. Since the crushed samples included grain sizes from 60 to 1000μ the possibility of turbulence having been present is very real. The effect of turbulence on electrokinetic phenomena is probably complex. One can expect an enhanced viscosity called eddy or turbulent viscosity, and this should act to lower the streaming potential according to 2.11 . The addition of an eddy

diffusion on top of the molecular diffusion could unbalance the Debye zone and cause it to expand, however, which would increase the zeta potential. Measurements were therefore undertaken at lower pressure gradients in order to reduce the turbulence effects. These measurements gave consistently higher streaming potentials but the inferred zeta potentials still seem too low. It is not clear that we have prevented turbulence even at pressures of only one-tenth of an atmosphere, and there are hints that higher streaming potentials would be obtained at even lower pressure gradients. Figure 8 shows some of these results. More work is needed to establish satisfactory methods of measuring zeta potentials, but at this point we have to stick with our model derived estimates of zeta potentials in the vicinity of 75 mv.

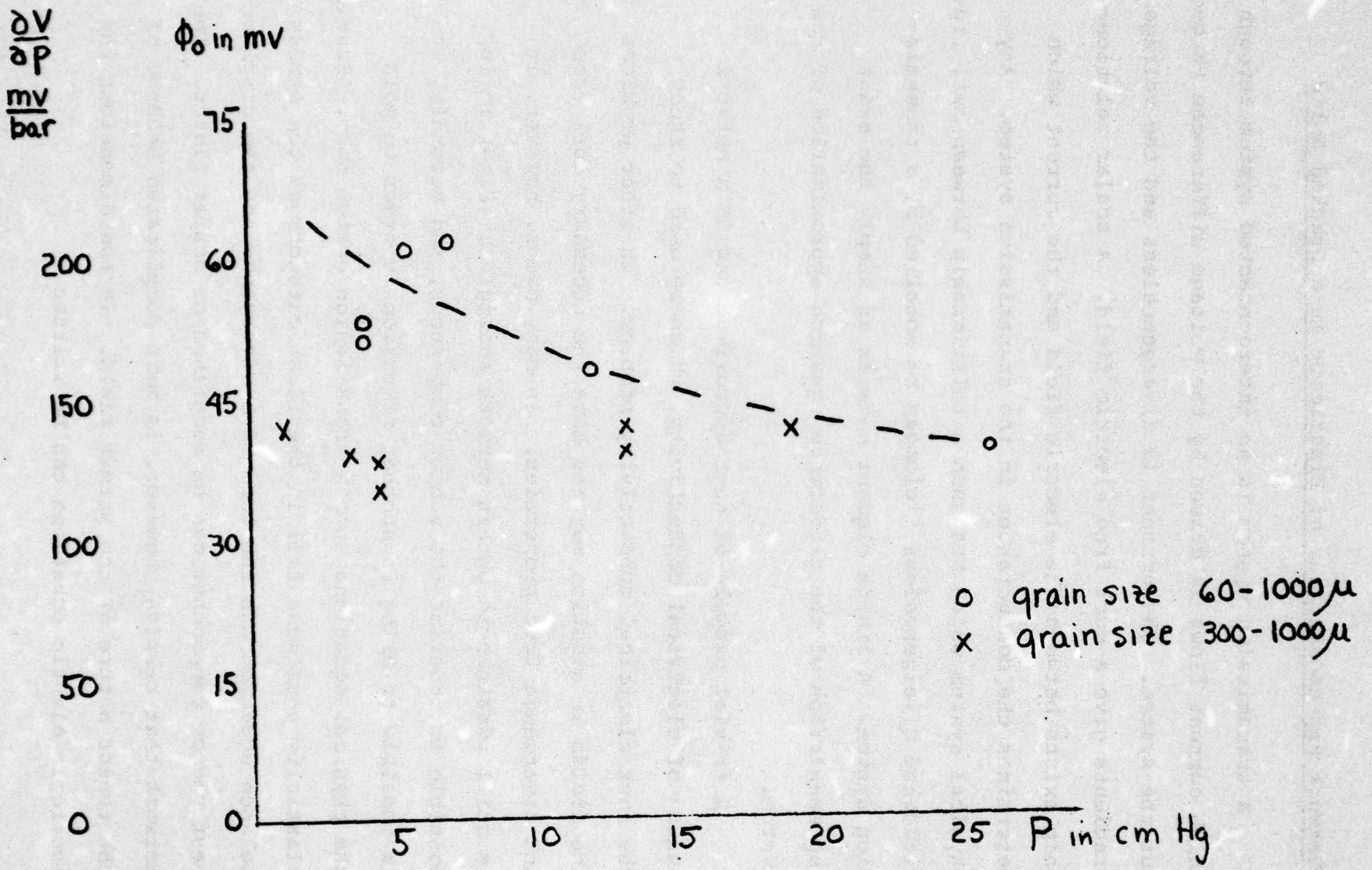

Fig 8 Streaming Potentials and Zeta Potentials in Tap Water on crushed Westerly Granite at low Pressures

III Network Representations of Elasticity in a Cracked Solid

A transmission system is an interconnected system through which current flows as driven by the voltage differences throughout the system. The current is divergenceless and the voltage gradients give a curl free electric field. A scalar relationship exists between the electric field and the current which determines the conductances in the transmission system. Any physical system which has such a relationship between curl free fields and divergenceless fields can be modelled by a transmission system. A finite element network is simply the exact representation of the difference equation approximation of the system.

A trivial example of such approximations is a network analog of electrical conductivity, which we used to study the rock electrical conductivity problem. In other problems the fields in question may not have the necessary curl free and divergence free properties. In many cases, however, it is still possible to obtain network analogies. First it is possible to redefine the vector components, and secondly, it is possible to bring in another dimension in order to mold the physical equations into a transmission system form. Static elasticity equations fall in the first category as the stress balance equation has the form of a divergence and the displacement vector components can be redefined as scalar fields. The network that results, however, is more complicated because of the tensor nature of the stress field. In two dimensions the isotropic elastic equations can be written

$$\begin{bmatrix} Txx \\ Tzx \end{bmatrix} = + \begin{bmatrix} \lambda+2\mu & 0 \\ 0 & \mu \end{bmatrix} \frac{\delta}{\delta x} \begin{bmatrix} Ux \\ Uz \end{bmatrix} + \begin{bmatrix} 0 & \lambda \\ \mu & 0 \end{bmatrix} \frac{\delta}{\delta z} \begin{bmatrix} Ux \\ Uz \end{bmatrix} \tag{3.1a}$$

$$\begin{bmatrix} Txz \\ Tzz \end{bmatrix} = + \begin{bmatrix} 0 & \mu \\ \lambda & 0 \end{bmatrix} \frac{\delta}{\delta x} \begin{bmatrix} Ux \\ Uz \end{bmatrix} + \begin{bmatrix} \mu & 0 \\ 0 & \lambda+2\mu \end{bmatrix} \frac{\delta}{\delta z} \begin{bmatrix} Ux \\ Uz \end{bmatrix} \tag{3.1b}$$

$$\frac{\delta}{\delta x} \begin{bmatrix} Txx \\ Tzx \end{bmatrix} + \frac{\delta}{\delta z} \begin{bmatrix} Txz \\ Tzz \end{bmatrix} = \begin{bmatrix} 0 \\ 0 \end{bmatrix} \tag{3.2}$$

Txx and Tzx represent x directed current variables and Txz and Tzz represent z directed current variables, while Ux and Uz are voltage variables. Txx, Txz, and Ux form one transmission system and Tzx, Tzz, and Uz form another one, but the two systems are coupled together by symmetric terms. The difference equation approximation will therefore lead to a two-level planer network. These networks without the intraconnections between levels are shown in Figure 9. The node points are assumed to lie on the boundaries of rectangular zones, each zone having its own elastic constants. The conductance elements between nodes are therefore averages of the elastic properties on the two sides of the boundary. The negative sign of these conductances arises from our convention of calling tension a positive stress. If the grid spacing is not square the vertically directed elements should be modified by the factor $\Delta x/\Delta z$ and the horizontally directed elements by the factor $\Delta x/\Delta z$. The cross coupling elements can be determined using circuits such as that shown in Figure 10. The result is shown in Figure 11. No modifications are needed for these elements when the spacing is not square.

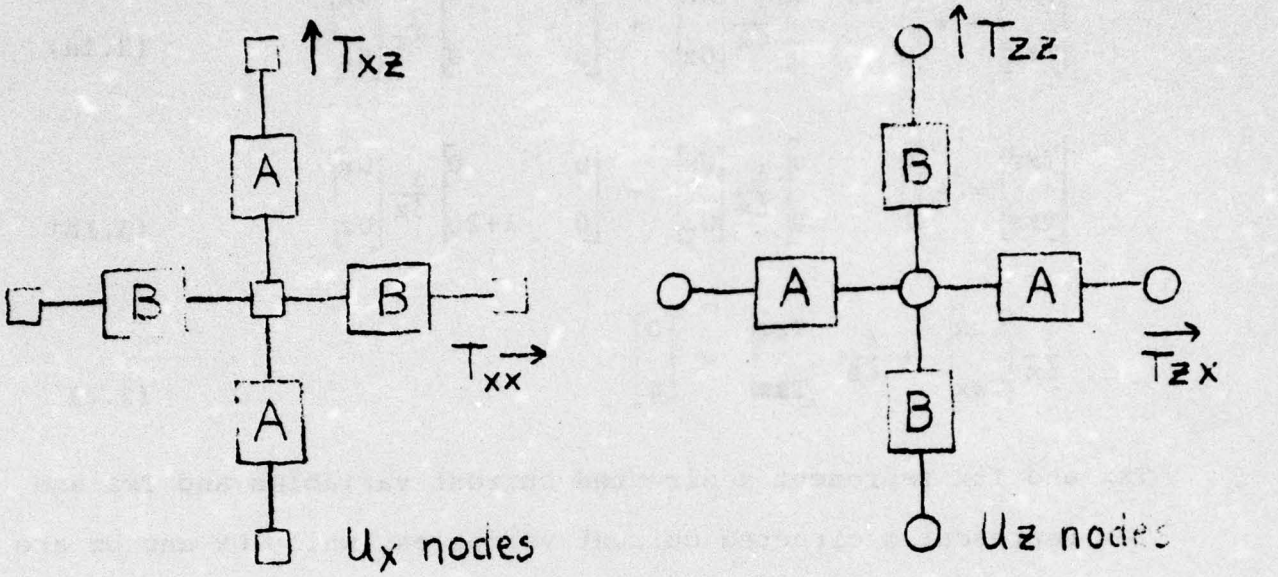

$A = -\Sigma\mu/2 \qquad B = -\Sigma(\lambda+2\mu)/4$

$\Sigma \equiv$ clockwise zone property + counter-clockwise property

Fig 9 Interconnections between u_x and u_z nodes

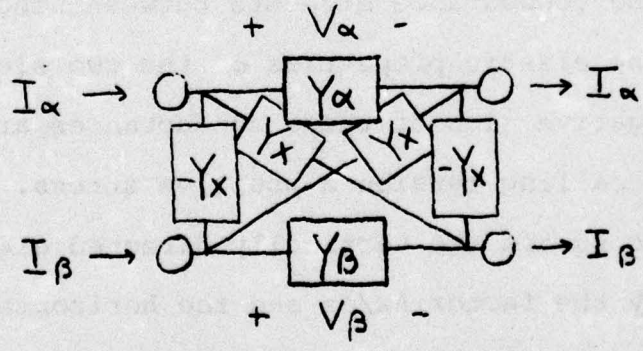

$$\begin{bmatrix} I_\alpha \\ I_\beta \end{bmatrix} = \begin{bmatrix} Y_\alpha & Y_x \\ Y_x & Y_\beta \end{bmatrix} \begin{bmatrix} V_\alpha \\ V_\beta \end{bmatrix}$$

Fig 10 Symetric Cross Coupling Circuit

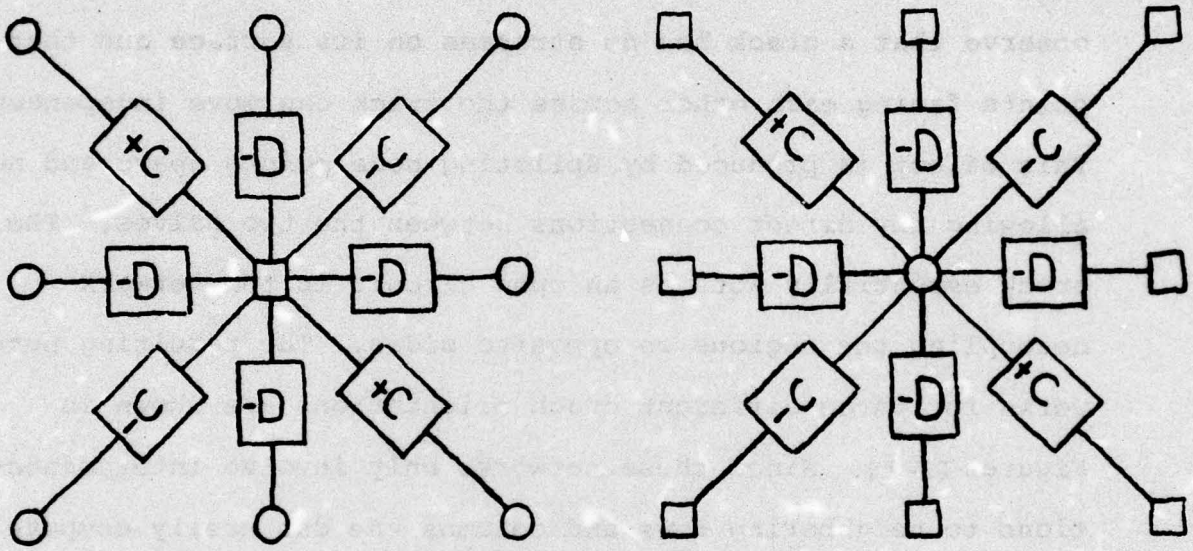

$C = (\lambda+\mu)/4 \qquad D = \Delta(\lambda-\mu)/4$

$\Delta \equiv$ clockwise zone property - counter-clockwise property

Fig 11 Intraconnections between u_x and u_z nodes

In order to investigate the role of cracks we need an efficient way to represent them in the network analog. In the electric problem this was achieved by having the network represent the crack contributions and ignoring the matrix which is a non-conductor. In the mechanical problem we must have both the crack and the matrix represented. This can be readily accomplished for a restricted set of crack orientations. We observe that a crack has no stresses on its surface and that points facing each other across the crack can move independently. This effect is produced by splitting node points apart and not allowing any direct connections between the two halves. The crack essentially acts as an open circuit in the network decoupling the regions on opposite sides. The resulting networks for three different crack orientations are shown in Figures 12-14. Since these networks only involve interconnections to neighboring rows and columns one can easily compute the network solutions by computing the network row admittance, a row at a time, starting from the bottom and working up. The Ux and Uz nodes of the same physical position can be considered as different nodes but of the same row.

If we define the interconnection conductance matrix of the M'th row as Y_x^{mm} and the intraconnection conductance matrix between the n'th and m'th rows as Y_z^{nm}, and the current coming into the m'th row from above as I_z^m, then we have

$$I_{zi}^n = \sum_j Y_{xij}^{nn}(V_i^n - V_j^n) + \sum_j Y_{zij}^{nm}(V_i^n - V_j^m) \qquad (3.3)$$

$$I_{zj}^m = \sum_i Y_{zij}^{nm}(V_i^n - V_j^m) \qquad (3.4)$$

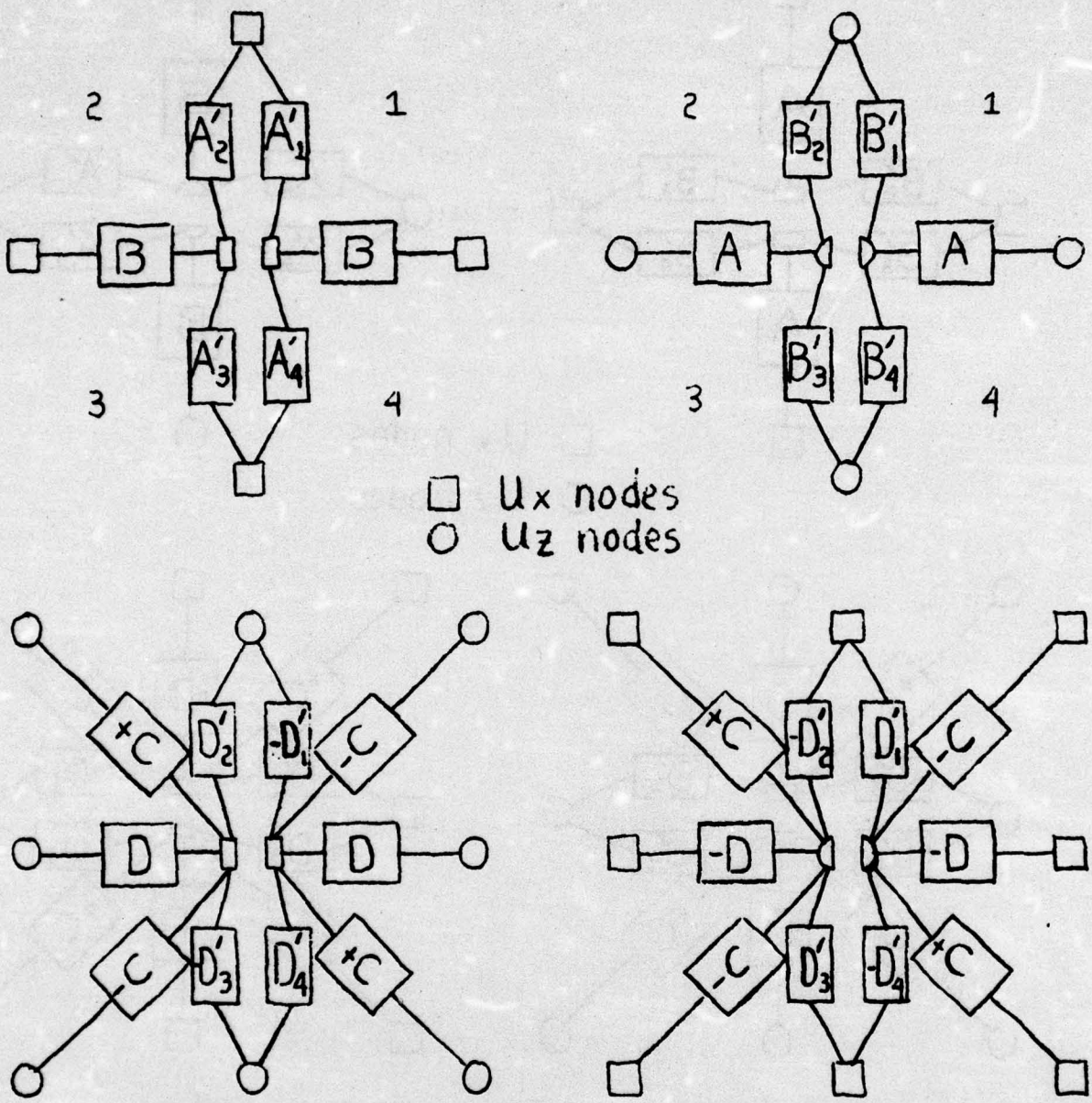

$A'_i = -\mu_i/2 \quad B'_i = -(\lambda+2\mu)_i/2 \quad D'_i = +(\lambda-\mu)_i/4$

Fig 12 Vertical Crack Representation

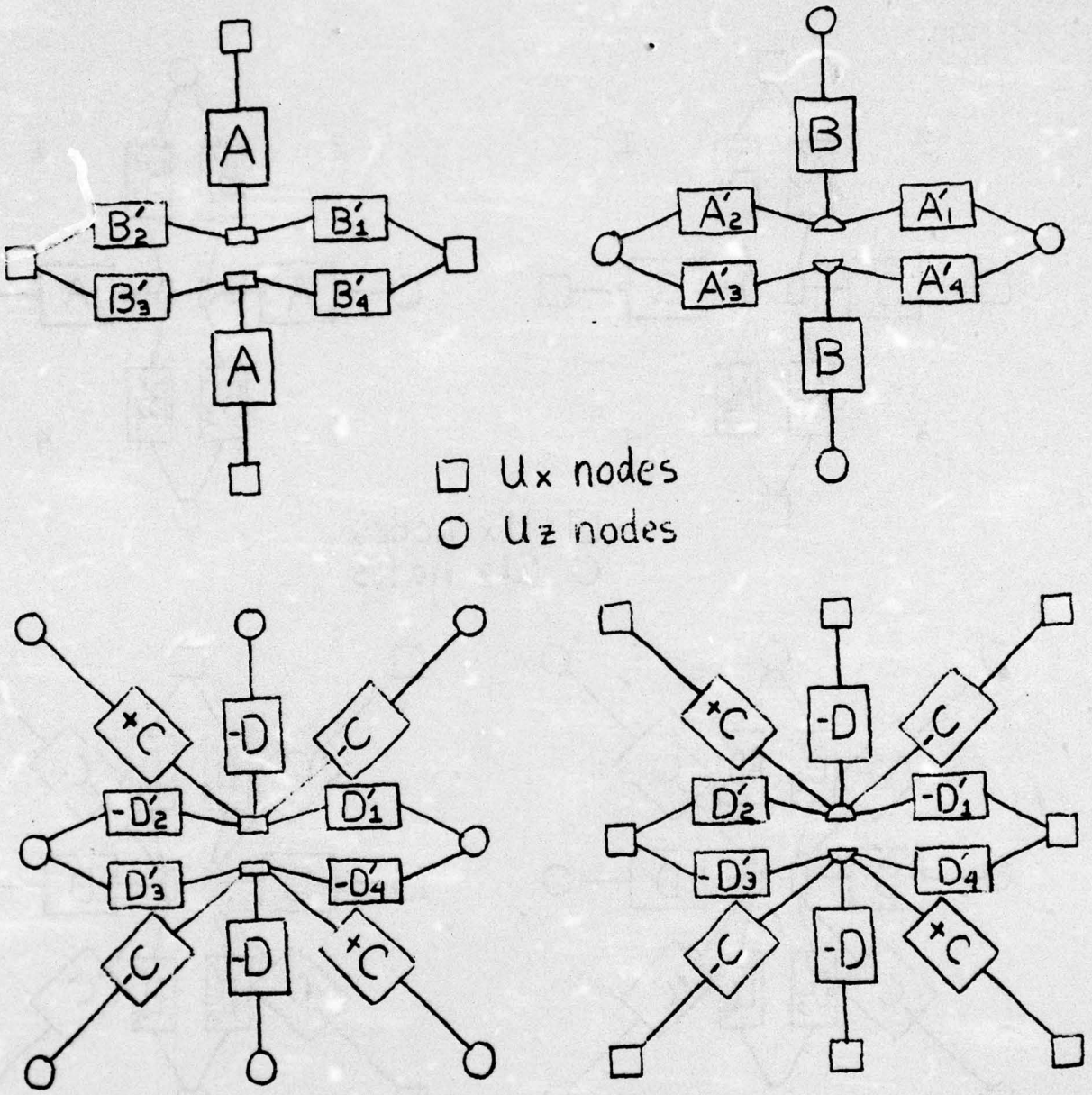

$$A'_i = -\mu_i/2 \quad B'_i = -(\lambda+2\mu)_i/2 \quad D'_i = +(\lambda-\mu)_i/4$$

Fig 13 Horizontal Crack Representation

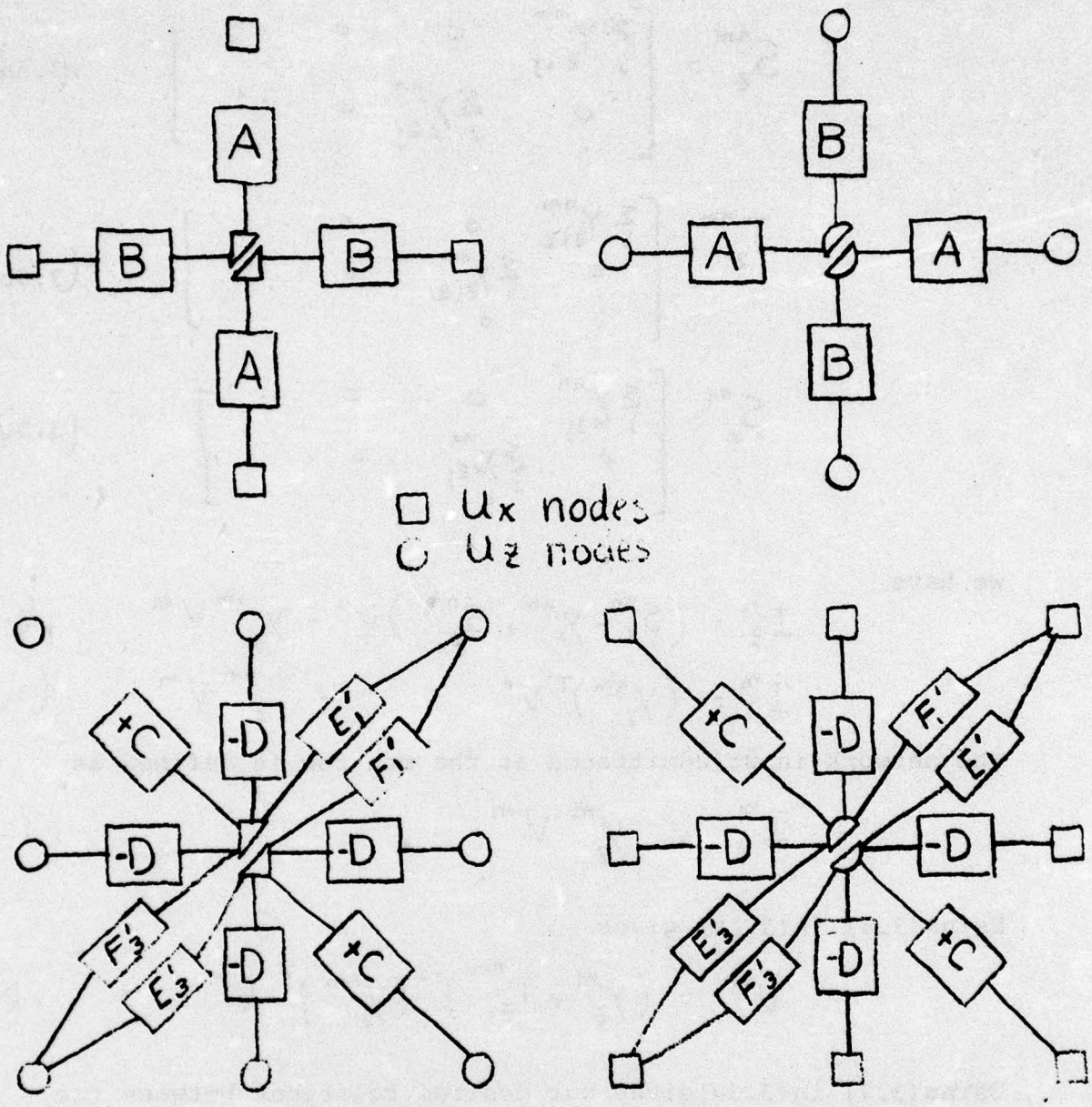

$E_i' = -\mu_i/4 \qquad F_i' = -\lambda_i/4$

Fig 14 Inclined Crack Representation

defining

$$S_z^{nm} = \begin{bmatrix} \sum_j Y_{z1j}^{nm} & 0 & 0 & \cdots \\ 0 & \sum_j Y_{z2j}^{nm} & 0 & \cdots \\ \vdots & \vdots & \vdots & \end{bmatrix} \qquad (3.5a)$$

$$T_z^{nm} = \begin{bmatrix} \sum_i Y_{zi1}^{nm} & 0 & 0 & \cdots \\ 0 & \sum_i Y_{zi2}^{nm} & 0 & \cdots \\ \vdots & 0 & & \end{bmatrix} \qquad (3.5b)$$

$$S_x^{nn} = \begin{bmatrix} \sum_j Y_{x1j}^{nn} & 0 & 0 & \cdots \\ 0 & \sum_j Y_{x2j}^{nn} & 0 & \cdots \\ \vdots & 0 & & \end{bmatrix} \qquad (3.5c)$$

we have

$$I_z^n = (S_x^{nn} - Y_x^{nn} + S_z^{nm})V^n - Y_z^{nm} V^m \qquad (3.3a)$$

$$I_z^m = (Y_z^{nm})^T V^n - T_z^{nm} V^m \qquad (3.4a)$$

The network input admittance at the mth row is defined as

$$I_z^m = Y_z^m V^m \qquad (3.6)$$

Using(3.6) in(3.4a) gives

$$V^m = (Y_z^m + T_z^{nm})^{-1} (Y_z^{nm})^T V^n \qquad (3.7)$$

Using(3.7) in(3.3a)gives our desired relations between the admittance matrix of one row and the admittance matrix of the previous row.

$$I_z^n = [S_x^{nn} - Y_x^{nn} + S_z^{nm} - Y_z^{nm}(Y_z^m + T_z^{nm})^{-1}(Y_z^{nm})^T]V^n \qquad (3.8)$$

or

$$Y_z^n = [S_x^{nn} - Y_x^{nn} + S_z^{nm} - Y_z^{nm}(Y_z^m + T_z^{nm})^{-1}(Y_z^{nm})^T] \qquad (3.8a)$$

Using(3.8a)one cascades up through the rows and from the final

Y_z one obtains the input currents given the applied voltage. These currents and voltages then can be used to work back down the network determining the voltages and currents in every row, using(3.7) and (3.8).

As an example of such calculations we numerically duplicate a common laboratory measurement, uniaxial loading of a rock sample. The friction between the rigid piston and the rock sample prevents any appreciable horizontal strain at the piston boundary while the sides of sample are unconstrained. This results in non-uniform stresses and the experimentalists go to great pains to overcome this effect. The numerical results of such a loading are shown in Figures 15 and 16. Numerically one could install an ideal material between the piston and the sample that would allow the rock sample to expand uniformly throughout the sample length.

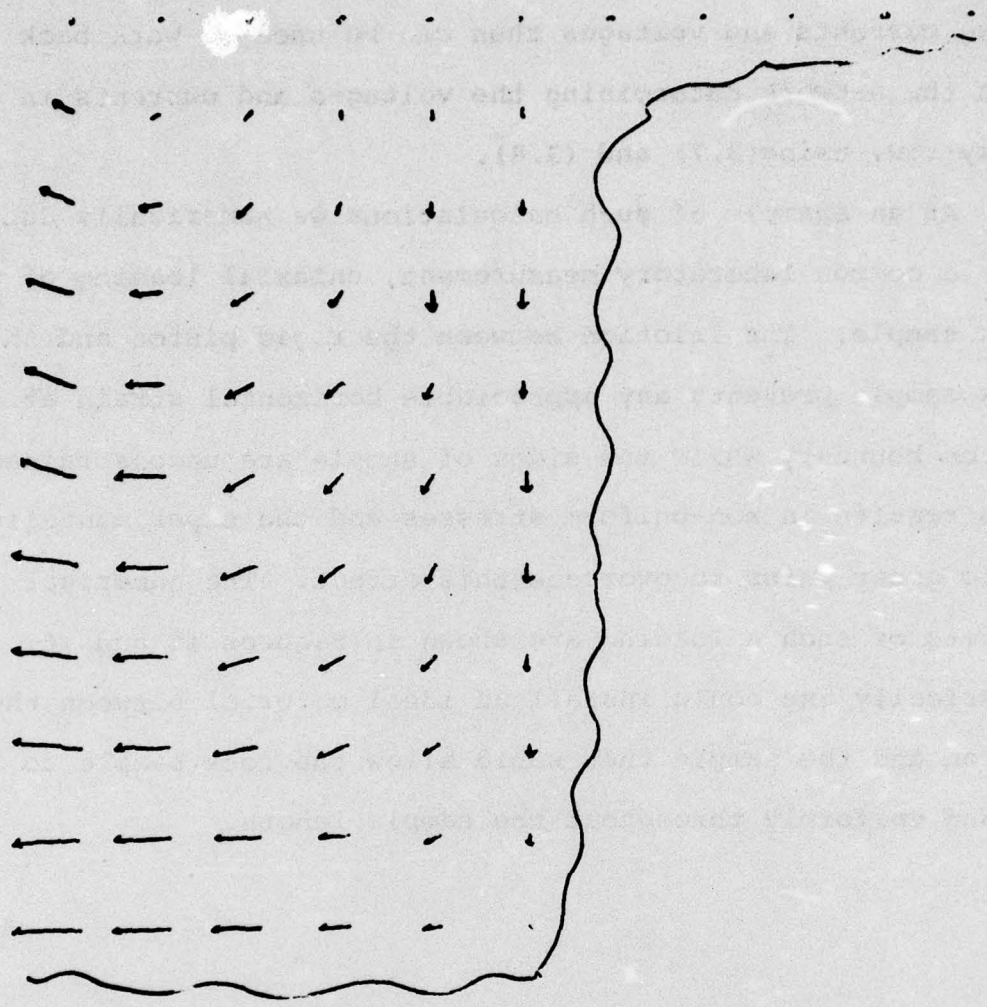

Fig 15 Displacement Field for Uniaxial Compression
confined at end surfaces
in Comparison To Uniform Shrinking in Vertical Direction
(upper left hand quadrant)

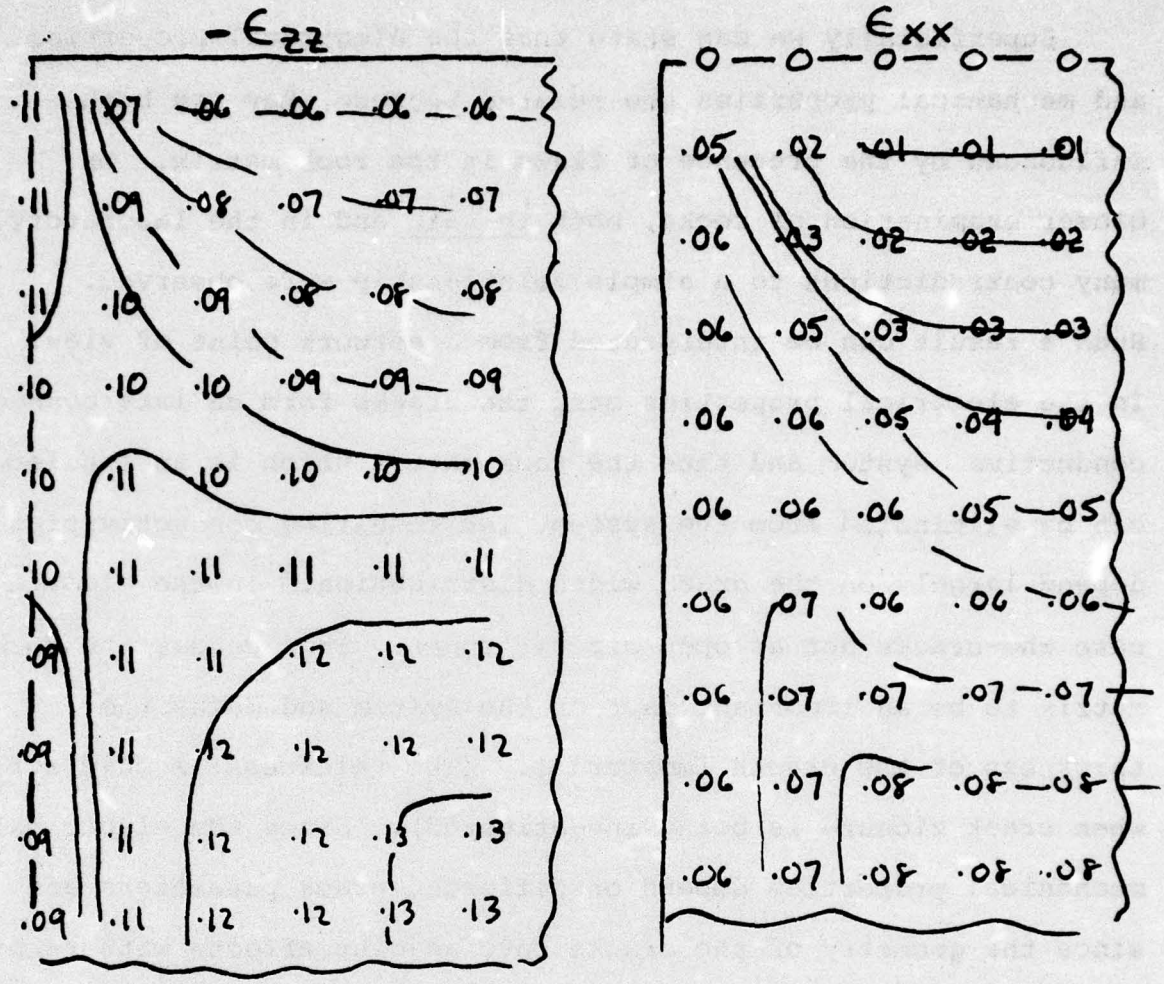

Fig 16 Elastic Strains in Uniaxially loaded Sample Confined at the Ends

(only upper left hand quarter of sample shown)

Conclusions

Superficially we can state that the electrical properties and mechanical properties are related because they are both influenced by the presence of flaws in the rock matrix. On closer examination of rocks, both in situ and in the laboratory, many contradictions to a simple relationship were observed. Such a result can be interpreted from a network point of view. In the electrical properties case the cracks form an interconnected conductive system and thus the rock matrix which is an insulator can be eliminated from the system. The resulting conductivities depend largely on the crack width distribution. In the elastic case the cracks act as open circuit zones. This causes the rock matrix to be an important part of the system and makes the thickness of the cracks immaterial. (The thickness is only a factor when crack closure is being investigated). Since the electrical and mechanical properties depend on different crack parameters and since the geometry of the cracks have adjoint effects with respect to the electrical and mechanical properties, it is not surprising that the interrelationship between these properties is not simple. Therefore, a good deal of apriori information is necessary before one property can be used to predict the other.

As a stressed rock approaches its failure point, the crack population goes through a dramatic change that causes important deviations in the rules that govern the conductivity of the cracks. At this point the empirical relationships between electrical and mechanical properties begin to follow a more consistent pattern. It is important, however, to develop a theoretical understanding of the role that this same crack population plays in the ultimate mechanical failure of a rock. Clearly some drastic change

in the crack interrelationships must occur. Simple concepts easily illustrated by network models explain the early crack development. Stress intensification factors associated with the presence of cracks cause local tensile stresses to occur when unequal principal stresses are applied even when both principal stresses are compressive. These local stresses cause the extension and development of cracks alligned with the maximum principal stress that is observed both electrically, as an anisotropic conductivity increase, and directly, by means of scanning electron microscope images. The failure, however, usually takes on the appearance of shear failure and is inclined to the principal stress axis. A critical question then is that concerning the role of the tension cracks in the failure. Is the failure actually shear failure or is it some organization of tension cracks that appears as shear failure or is it a combination of these two effects? The mechanical calculations are not simple as the cracks seem to be completely interconnected and calculations such as the network calculations are necessary to deal with these geometries. We believe the association of intense tension crack development with failure is not coincidental and that the second or third hypothesis must be operative. This then would justify a close correspondence between electrical and mechanical properties near failure. The simple network calculations that we are attempting must be expanded, however, perhaps by extensions of our embedded network concepts as used in the development of a theory of electrical conductivity, since the three dimensional aspects of the problem are extremely important, but brute force modelling in three dimensions is still too laborious to be practical.

References

Brace, W.F., J.B. Walsh, and W.T. Frangor, 1968. Permeability of granite under high pressure, Jour. of Geophys. Res., 73, 2225-2236.

Batzle, M.L., 1976. personal communication.

Hadley, K., personal communication, 1975.

Hadley, K., Dilatancy: Further Studies in Crystalline Rock, Ph. D. Thesis, M.I.T., 1975.

Madden, T.R., 1974, Near surface electrical properties of rocks as a guide to mechanical properties, final report AFCRL-TR-75-0179.

Acknowledgements

Our studies have greatly benefitted from special help we received from several individuals. Kate Hadley reorganized her crack data in order to get us the information we needed for tests of our conductivity theories. Michael Batzle made available for us his permeability measuring equipment for our surface conductivity studies. Olu Angulsoye shared some of his streaming potential data on jointed rock samples. We also wish to acknowledge the important contributions of Professor Bill Brace who is always ready to assist us in measurements and provide insights about rock structures.

Personnel Involved in Reported Studies

Theodore R. Madden, Principal Investigator

Earl Williams

Publications Resulting from Project Studies

Madden, T.R., 1976. Random networks and mixing laws, Geophys., 41, 1104-1125.